

Iterative approach to line-shape calculations based on the transport-relaxation equation

P. Wcisło,* A. Cygan, D. Lisak, and R. Ciuryło

*Institute of Physics, Faculty of Physics, Astronomy and Informatics, Nicolaus Copernicus University,
Grudziadzka 5, 87-100 Torun, Poland*

(Received 13 April 2013; published 24 July 2013)

The iterative approach to the line-shape calculations from the transport-relaxation equation was modified to allow its application for low pressures down to the Doppler limit. In our approach functions and operators are decomposed in the Burnett basis. This technique was applied to experimental data presenting the consistency between the line-shape model and measured spectrum corresponding to a signal-to-noise ratio higher than 9×10^4 . Implications for precise molecular spectroscopy as well as for Doppler-width thermometry and spectroscopic Boltzmann constant determination are discussed.

DOI: [10.1103/PhysRevA.88.012517](https://doi.org/10.1103/PhysRevA.88.012517)

PACS number(s): 32.70.Jz

I. INTRODUCTION

Realistic line-shape calculations, which can go beyond analytical models [1–8], require numerical solutions of the transport-relaxation equation with *ab initio* in spirit collision operator derived from interaction potential [9–17]. The most common methods of numerical solving of the transport-relaxation equation are based on the direct discretization of the velocity space [18–21] or decomposition of operators and functions in some basis, typically Burnett functions [9–14, 17, 22–24]. These two approaches lead to a conversion of an integral transport-relaxation equation into a system of linear algebraic equations [10, 13, 17, 19, 23]. They appear effective for line-shape calculations and experimental spectra interpretation at middle and high pressures of perturber gases [11, 20, 24–31]. However, it was reported that the accuracy of these approaches dramatically falls down for a low-pressure range, where the Doppler broadening is dominant [14, 21, 22, 28, 31, 32]. Very recently, Tran *et al.* [21] used first-order approximation to overcome this problem, see also [33], exploring analogy between Dicke narrowing and line mixing [34].

More advanced line-shape models, which are able to handle both Dicke narrowing and speed-dependent effects, are strongly desired for high-quality spectra interpretation in the low-pressure range. First of all, it was shown that data analysis for experiments on optical determination of the Boltzmann constant [35–38] requires spectral line profile models providing relative accuracy of order of 10^{-6} for pressures down to a few Pa [39–41]. Very recently, Moretti *et al.* [42] demonstrated spectroscopic determination of the Boltzmann constant with relative accuracy at a level of 10^{-5} , in which Dicke narrowing and speed-dependent effects were taken into account simultaneously. In addition, a cavity ring-down spectroscopy, recently allowed to obtain extremely high signal-to-noise ratio (SNR) of line-shape measurements for very low pressures [43], that together with other experimental achievements [44–50] opens a door for line-shape models tests with unprecedented accuracy.

In this paper we present an iterative method of the transport-relaxation equation solving applicable to a wide range of pressures including very low pressures down to

the Doppler limit. We modified an iterative approach given by Nienhuis [33] and implemented for the Keilson-Storer model by Shapiro *et al.* [18], which at the low-pressure regime appears ineffective. It is shown that this technique is able to provide spectral line profiles with relative accuracy better than 10^{-6} for a number of physical models such as Gauss profile, Voigt profile, Nelkin-Ghatak profile, Galatry profile, Billiard-Balls profile, Blackmore profile, and also speed-dependent versions of these profiles. Finally, we have applied our iterative technique to a high SNR spectral line profile of the R7 Q8 $^{16}\text{O}_2$ B-band rovibronic transition [43] presenting the consistency between the line-shape model and experimental data corresponding to SNR higher than 9×10^4 .

II. ITERATIVE APPROACH TO TRANSPORT-RELAXATION EQUATION

The problem of spectral line profile determination within the impact approximation can be handled in terms of the stationary solution of the transport-relaxation equation [13, 17, 51]. It is sometimes convenient to factor out the Maxwellian velocity distribution $f_m(\vec{v})$ from this equation and transform it to the following form [10, 13–15, 22]:

$$1 = -i(\omega - \omega_0 - \vec{k} \cdot \vec{v})h(\omega, \vec{v}) - \hat{S}^f h(\omega, \vec{v}), \quad (1)$$

where \vec{v} is the absorber velocity, \vec{k} is the wave vector, ω is the light frequency, and the ω_0 is the frequency of the unperturbed isolated transition. The \hat{S}^f operator describes collisions and relaxation processes. The physical meaning of the $h(\omega, \vec{v})$ function is that quantity $f_m(\vec{v})h(\omega, \vec{v})$ is proportional to the optical coherence velocity distribution and it allows us to calculate the absorption line profile $I(\omega)$ as a following integral:

$$I(\omega) = \frac{1}{\pi} \text{Re} \int f_m(\vec{v})h(\omega, \vec{v})d^3\vec{v}. \quad (2)$$

The Maxwellian velocity distribution is $f_m(\vec{v}) = (\sqrt{\pi}v_m)^{-3} e^{-(v/v_m)^2}$, where the most probable speed $v_m = \sqrt{2k_B T/m_1}$, and k_B , T , and m_1 are the Boltzmann constant, the temperature, and the absorber mass, respectively.

In our approach the last term in Eq. (1) is treated as a small correction and then we derive the iterative perturbation stencil from Eq. (1). However, for a zero detuning ($\omega - \omega_0 - \vec{k} \cdot \vec{v}$) affected by the Doppler shift the small correction becomes dominant and the iterative scheme fails. To ensure the

*piotr.wcislo@fizyka.umk.pl

stability of the iterative perturbation process and to control its convergence we introduced to Eq. (1) a constant nonphysical parameter Γ_{num} ,

$$1 = [\Gamma_{\text{num}} - i(\omega - \omega_0 - \vec{k} \cdot \vec{v})]h(\omega, \vec{v}) - (\Gamma_{\text{num}} + \hat{S}^f)h(\omega, \vec{v}). \quad (3)$$

A simple algebraic manipulation gives then an iterative perturbation scheme,

$$h^{(n+1)}(\omega, \vec{v}) = a(\omega, \vec{v}) + \hat{A}(\omega)\hat{B}h^{(n)}(\omega, \vec{v}), \quad (4)$$

where the $a(\omega, \vec{v})$ function is given by the following formula:

$$a(\omega, \vec{v}) = \frac{1}{\Gamma_{\text{num}} - i(\omega - \omega_0 - \vec{k} \cdot \vec{v})}. \quad (5)$$

Note that Γ_{num} is a nonphysical constant, which determines the stability and the convergence of the method. This quantity will affect the width of the line profile only in a few first iteration steps and should not be confused with the collisional width of the spectral line. The \hat{A} operator acts as a simple multiplication by the $a(\omega, \vec{v})$ function,

$$\hat{A}(\omega)h(\omega, \vec{v}) = a(\omega, \vec{v})h(\omega, \vec{v}), \quad (6)$$

and the \hat{B} operators are defined as

$$\hat{B} = \hat{S}^f + \Gamma_{\text{num}}. \quad (7)$$

To proceed with the iterative process given by Eq. (4) we assumed that $h^{(0)}(\omega, \vec{v}) = 0$. For further calculations it is convenient to expand $a(\omega, \vec{v})$ with respect to $(x \cos \theta)$,

$$a(\omega, \vec{v}) = \frac{1}{\omega_D} \sum_{j=1}^{\infty} \frac{(-i)^{j-1}}{[\Gamma_{\text{num}}/\omega_D - i(\omega - \omega_0)/\omega_D]^j} (x \cos \theta)^{j-1}, \quad (8)$$

where $\omega_D = kv_m$, $x = |\vec{v}|/v_m$, and θ is an angle between \vec{k} and \vec{v} . The convergence of this series for the required range of x can be achieved by an appropriate choice of Γ_{num} .

III. SOLUTION IN THE BURNETT BASIS

It is convenient to decompose operators \hat{A} , \hat{B} and functions $a(\omega, \vec{v})$ and $h^{(n)}(\omega, \vec{v})$ in the Burnett basis $\{\phi_s(\vec{v})\}$ [14,22,52]. Using notation of [13,14] the scalar product can be defined as $\langle \phi_s | \phi_{s'} \rangle = \int d^3\vec{v} f_m(\vec{v}) \phi_s(\vec{v}) \phi_{s'}(\vec{v}) = \delta_{ss'}$ and the first basis element is assumed to be a constant function $\phi_0(\vec{v}) = 1$. The integral equation (4) can be converted to a simple algebraic equation,

$$\underline{c}^{(n+1)}(\omega) = \underline{a}(\omega) + \mathbf{A}(\omega) \cdot \mathbf{B} \cdot \underline{c}^{(n)}(\omega), \quad (9)$$

where elements of columns $\underline{c}^{(n)}(\omega)$ and $\underline{a}(\omega)$ are defined as $c_s^{(n)}(\omega) = \langle \phi_s(\vec{v}) | h^{(n)}(\omega, \vec{v}) \rangle$ and $a_s(\omega) = \langle \phi_s(\vec{v}) | a(\omega, \vec{v}) \rangle$. Elements of the matrices $\mathbf{A}(\omega)$ and \mathbf{B} are defined as $A_{s,s'}(\omega) = \langle \phi_s(\vec{v}) | \hat{A}(\omega) | \phi_{s'}(\vec{v}) \rangle$ and $B_{s,s'} = \langle \phi_s(\vec{v}) | \hat{B} | \phi_{s'}(\vec{v}) \rangle$ [note that the $\underline{a}(\omega)$ vector is the first column of the symmetric matrix $\mathbf{A}(\omega)$]. The Burnett functions $\phi_s(\vec{v})$ are identified by two numbers; hence the subscript s should be regarded as a pair of indexes $\{n, l\}$ such that $n = 0, \dots, N_{\text{max}}$ and $l = 0, \dots, L_{\text{max}}$, where N_{max} and L_{max} determines the basis size, which is equal to $N_{\text{max}} L_{\text{max}}$. Equation (8) in the matrix form can be written as

$$\mathbf{A}(\omega) = \frac{1}{\omega_D} \sum_{k=0}^{\infty} \frac{(-i)^k}{[\Gamma_{\text{num}}/\omega_D - i(\omega - \omega_0)/\omega_D]^{k+1}} \mathbf{P}_k. \quad (10)$$

For the purpose of numerical calculations in Eq. (10) the finite sum with $k = 0, \dots, K_{\text{max}}$ is used. Usually, for $\Gamma_{\text{num}}/\omega_D \approx 30$ this sum can be truncated at $K_{\text{max}} = 10$. The \mathbf{P}_k matrices are given by the following expression:

$$\begin{aligned} [\mathbf{P}_k]_{n_1, l_1; n_2, l_2} &= \sqrt{\frac{n_1! n_2! (2l_1 + 1)(2l_2 + 1)}{\Gamma(n_1 + l_1 + 3/2) \Gamma(n_2 + l_2 + 3/2)}} \text{mod}(k + l_1 + l_2 + 1, 2) \frac{1}{2^{l_1 + l_2 - 1}} \\ &\times \left[\sum_{i=0}^{\lfloor l_1/2 \rfloor} \sum_{j=0}^{\lfloor l_2/2 \rfloor} \frac{(-1)^{i+j}}{k + l_1 + l_2 - 2i - 2j + 1} \binom{l_1}{i} \binom{2l_1 - 2i}{l_1} \binom{l_2}{j} \binom{2l_2 - 2j}{l_2} \right] \frac{1}{2} \Gamma(n_1 + l_1 + 3/2) \\ &\times \Gamma(n_2 + l_2 + 3/2) \sum_{\tilde{i}=0}^{n_1} \sum_{\tilde{j}=0}^{n_2} \frac{(-1)^{\tilde{i}+\tilde{j}} \Gamma(\frac{3+k+l_1+l_2+2\tilde{i}+2\tilde{j}}{2})}{\tilde{i}! \tilde{j}! (n_1 - \tilde{i})! (n_2 - \tilde{j})! \Gamma(\tilde{i} + l_1 + 3/2) \Gamma(\tilde{j} + l_2 + 3/2)}. \end{aligned} \quad (11)$$

In this equation $\Gamma(\dots)$ is a gamma function (not to be confused with the pressure broadening). It should be noted that the form of the \mathbf{P}_k matrix is an intrinsic feature of the iterative stencil Eq. (9) with the decomposition in the Burnett basis and it does not depend on the parameters of the physical system and therefore the set of \mathbf{P}_k matrices has to be evaluated only once for all possible spectral line-shape models handled by Eq. (1).

According to Eq. (7) the \mathbf{B} matrix is a sum of the identity matrix multiplied by Γ_{num} and the \mathbf{S}^f matrix, which describes collisions and relaxations. The problem of \mathbf{S}^f matrix determination was analyzed in the literature. The velocity-changing

contribution to \mathbf{S}^f was discussed for the Keilson-Storer model [19,24] (also a hard-collisions model in the limit case), for the billiard-balls model (also a soft-collisions model in the limit case) [14,22,52], and for the inverse-power potential model [17,52]. Analytical as well as numerical approaches to the determination of dephasing contribution to \mathbf{S}^f , leading to the speed-dependent collisional broadening and shifting [53], were presented in [14,17,19,24]. Finally, the line-shape profile [Eq. (2)] can be written as

$$I(\omega) = \frac{1}{\pi} \text{Re} \langle \phi_0(\vec{v}) | h(\omega, \vec{v}) \rangle = \frac{1}{\pi} \text{Re} [c_0(\omega)]. \quad (12)$$

Evaluation of a single point from the profile $I(\omega)$ requires one complex multiplication of $(N_{\max}L_{\max}) \times (N_{\max}L_{\max})$ square matrices and n complex multiplications of $(N_{\max}L_{\max}) \times (N_{\max}L_{\max})$ square matrix by $N_{\max}L_{\max}$ column, where n is a number of required iterative steps. Computations needed to proceed our iterative calculations can be easily parallelized, since they need only the matrix multiplication procedure; see Eq. (9).

IV. NUMERICAL CONVERGENCE

The convergence and accuracy of the iterative approach outlined in the previous section need to be examined. We compared the spectral line profiles generated with the proposed iterative method (denoted by I_{iter}) and an exact reference profile (denoted by I_{exact}). Figure 1(a) shows a whole profile generated with the iterative method, while Figs. 1(b)–1(e) show the differences between the iterative profiles and an

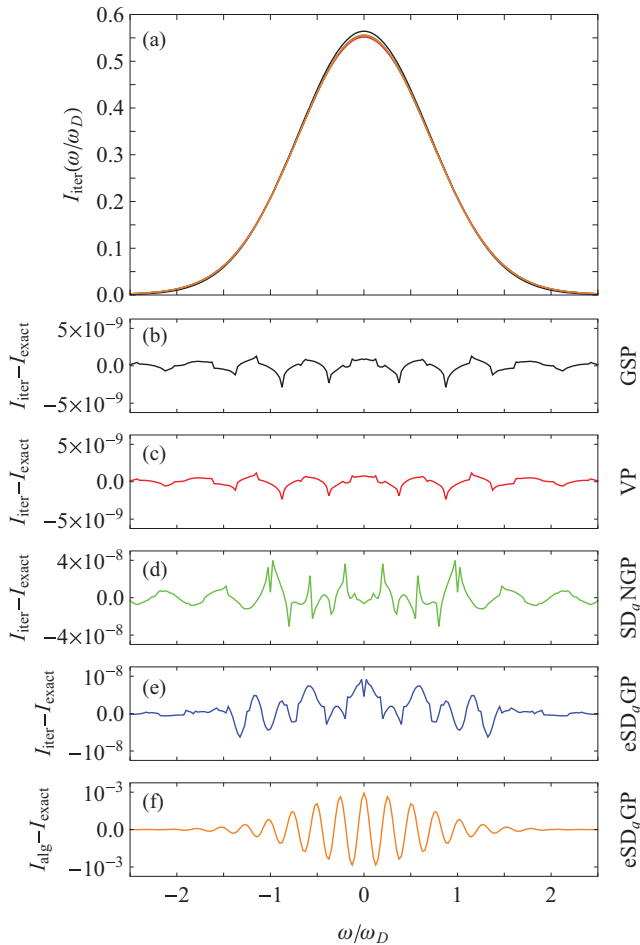


FIG. 1. (Color online) (a) Spectral line profiles generated with iterative method. (b)–(e) Differences between profiles generated with iterative method and more accurate reference profiles. (f) Differences between profile generated with diagonalization method and more accurate reference profiles. Color designation of line-shape models in chart (a) is the same as in (b)–(f). These results were obtained for $\Gamma/\omega_D = 0.02$, $v_{\text{opt}}/\omega_D = 0.01$, $a_W = 0.1$, $\Delta = 0$, $a_S = 0$, $N_{\max} = L_{\max} = K_{\max} = 25$, and $\Gamma_{\text{num}}/\omega_D = 30$.

exact reference profile for the cases of Gauss profile (GSP), Voigt profile (VP), speed-dependent Nalkin-Ghatak profile (SD_qNGP) [2], and exact speed-dependent Galatry profile (eSD_qGP) [54], respectively (in the last two cases the subscript q indicates that the quadratic speed dependence was utilized). To generate SD_qNGP [2] we used analytical expressions described in [2,3], which are based on calculations of the speed-dependent Voigt profile (SDVP) [53]. For a quadratic speed dependence SDVP can be also calculated from expressions given in [55]; however, this approach was not implemented here. Evaluation of eSD_qGP was carried out using analytical expressions derived in [54]. In this section the profiles were calculated for reduced collisional broadening $\Gamma/\omega_D = 0.02$, reduced collisional narrowing parameter $v_{\text{opt}}/\omega_D = 0.01$, collisional shift $\Delta = 0$, and the parameters controlling the speed dependence of the collisional width $a_W = 0.1$ and shift $a_S = 0$, according to notation in [14]. The parameter controlling the stability of the iterative method was $\Gamma_{\text{num}}/\omega_D = 30$, the basis dimensions were $N_{\max} = L_{\max} = 25$ and the upper limit of the sum from Eq. (10) was $K_{\max} = 25$. To show an advantage of the iterative approach over other alternative methods, in the range of low pressures, the difference between eSD_qGP generated from an exact solution of algebraic representation of Eq. (1) in a truncated basis like in [14] (we will refer to it as the “algebraic” method and denote the corresponding profile by I_{alg}) and from an accurate reference method [54] (denoted by I_{exact}) is presented in Fig. 1(f). Comparing Figs. 1(e) and 1(f) one may observe that the iterative method provides the accuracy of five orders of magnitude better than the algebraic method (it should be noted that in both cases the size of Burnett function bases were the same: $N_{\max} = L_{\max} = 25$). Moreover, the accuracy of the algebraic method deteriorates by another several orders of magnitude with the further decrease of the pressure, while the accuracy of the iterative solution remains very high or even slightly grows up [compare with the limit case of zero pressure shown in Fig. 1(b)].

The convergence of the iterative perturbation process is presented in Fig. 2 for eSD_qGP, for reduced detuning $(\omega - \omega_0)/\omega_D = 1$ [all parameters of the profile are the same as in Fig. 1(e)]. The black line represents the absolute value of the difference between the iterative solution and an accurate reference [54]. After about 300 steps the error of iterative solutions decreased by more than nine orders of magnitude. The speed at which this error approaches its minimum depends on the Γ_{num} parameter. Increase of Γ_{num} value leads to slower convergence, but also to higher stability of the method. We found that the value of $\Gamma_{\text{num}}/\omega_D = 30$ provides an accurate result in a wide range of model parameters; however, we suppose that the problem of the choice of Γ_{num} still can be optimized. After reaching the minimum the error of iterative solution usually increases. It is caused by the fact that the iterative solution starts to approach the algebraic solution in a truncated basis, which is not able to properly reconstruct an exact solution. Therefore, there is a need to find a criterion, which will say when to stop the iteration procedure.

One may observe that as long as the iterative process is convergent the absolute value of the corrections to the line-shape profiles $|\Delta I_{\text{iter}}^{(n)}(\omega)| = |I_{\text{iter}}^{(n)}(\omega) - I_{\text{iter}}^{(n-1)}(\omega)|$ should

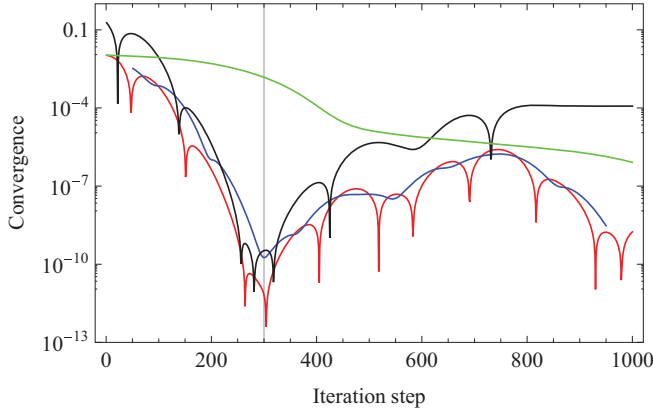


FIG. 2. (Color online) Convergence of the iterative process is illustrated by the absolute value of the difference between the iterative solution and more accurate reference profile $|I_{\text{iter}}^{(n)}(\omega) - I_{\text{exact}}(\omega)|$ as a function of the number of iterative steps; see the black line. The red line represents the absolute value of the correction to the line-shape profiles at n th step $|\Delta I_{\text{iter}}^{(n)}(\omega)| = |I_{\text{iter}}^{(n)}(\omega) - I_{\text{iter}}^{(n-1)}(\omega)|$. The blue curve shows a mean correction defined as $|\overline{\Delta I_{\text{iter}}^{(n)}(\omega)}| = \frac{1}{101} \sum_{i=-50}^{50} |\Delta I_{\text{iter}}^{(n+i)}(\omega)|$ and the minimum of this function is indicated by a gray vertical line. The green line represents the $|\Delta \underline{c}^{(n)}(\omega)|$ correction; see Eq. (13). These results were obtained for eSD_qGP for $(\omega - \omega_0)/\omega_D = 1$, $\Gamma/\omega_D = 0.02$, $\nu_{\text{opt}}/\omega_D = 0.01$, $a_W = 0.1$, $\Delta = 0$, $a_S = 0$ and $N_{\text{max}} = L_{\text{max}} = K_{\text{max}} = 25$, $\Gamma_{\text{num}}/\omega_D = 30$.

decrease with the iterative steps; hence the simplest idea for the stopping criterion is to look for the minimum of the $|\Delta I_{\text{iter}}^{(n)}(\omega)|$ correction. However, $\Delta I_{\text{iter}}^{(n)}(\omega)$ does not monotonically decrease but rather oscillate around the exact solution and the amplitude of this oscillation decreases monotonically; see the red curve in Fig. 2. Therefore, it is better to look for the minimum of the mean correction defined as $|\overline{\Delta I_{\text{iter}}^{(n)}(\omega)}| = \frac{1}{101} \sum_{i=-50}^{50} |\Delta I_{\text{iter}}^{(n+i)}(\omega)|$; see the blue curve in Fig. 2 (we arbitrarily chose to average over 101 points and we also found that the value of this parameter has a small impact on the line-shape accuracy).

Comparing the iterative and the algebraic methods a question about the uniqueness of decomposition in the Burnett basis arises. In both cases the same transport-relaxation equation [Eq. (1)] is considered and the solutions are represented in the Burnett basis. One could expect that for the same basis dimensions these solutions should be the same or almost the same (possible discrepancies may be caused by different numerical errors intrinsic for both approaches) and we found that it is true for iterations approaching an infinite number of steps. However for truncated iterations, according to Figs. 1(e) and 1(f), they give dramatically different accuracies. We should emphasize that it is not caused by the numerical errors but rather because that for both methods the whole issue is, in fact, defined differently.

Clearly, the Gaussian distribution related to a zero pressure limit is present in the term $a(\omega, \vec{\nu})$ under a convolution with the Lorentz profile having the width Γ_{num} . During the iterative process this Gaussian contribution is recovered. Around the minimum shown in Fig. 2 this recovery is the best in the $c_0^{(n)}(\omega)$ term. After this minimum $c_0^{(n)}(\omega)$ approaches the exact

solution of the truncated algebraic problem and the information about the Gaussian distribution contained in $a(\omega, \vec{\nu})$ is lost.

The algebraic technique of line-shape calculations is based on the solution to the system of linear coupled equations [see Eq. (2) in [14]], in which we look for all elements of the $\underline{c}(\omega)$ column simultaneously, such that we may optimally reproduce the whole $h(\omega, \vec{\nu})$ function in the truncated basis set. While in the iterative technique of line-shape calculations we are rather focused only on the first element of the $\underline{c}(\omega)$ column and the iteration process is proceeded only as long as the $c_0(\omega)$ converges. As can be seen from Eq. (12), the basis function $\phi_0(\vec{\nu}) = 1$ and $c_0(\omega)$ coefficient play a central role for the line-shape calculations. The success of the iterative approach proposed here depends on properties of the basis set and the collisional operator \hat{S}^f . It is important that the matrix $\mathbf{A}(\omega) \cdot \mathbf{B}$ from Eq. (9), in the Burnett basis representation, couples $c_s(\omega)$ coefficients with significantly different n and l indexes very weakly. Therefore, the iterative calculations of $c_0(\omega)$ are not affected by the basis truncation, even for a large number of iterative steps.

To illustrate how the whole $\underline{c}(\omega)$ vector evolve during the iterative process we plotted in Fig. 2, as a green line, a quantity similar to the absolute value of the correction to the line-shape profile $|\Delta I_{\text{iter}}^{(n)}(\omega)|$, but referring to the whole $\underline{c}(\omega)$ column, which we defined as

$$|\Delta \underline{c}^{(n)}(\omega)| = \frac{1}{\pi} |\underline{c}^{(n)}(\omega) - \underline{c}^{(n-1)}(\omega)|. \quad (13)$$

The results from Figs. 1 and 2 were generated for the case of low pressure ($\Gamma/\omega_D = 0.02$ and $\nu_{\text{opt}}/\omega_D = 0.01$); however it has been tested that for higher as well as lower pressures (down to $\Gamma/\omega_D = \nu_{\text{opt}}/\omega_D = 0$) the accuracy of the iterative solution is similar or better, as in the case of the Gauss profile in Fig. 1(b).

V. APPLICATION FOR MOLECULAR SPECTROSCOPY DATA ANALYSIS

In this section the application of the iterative approach in low-pressure experimental data analysis is presented. Figure 3(a) shows a high SNR spectral line profile of the R7 Q8 ¹⁶O₂ B-band rovibronic transition measured with a Pound-Drever-Hall-locked (PDH) frequency-stabilized cavity ring-down spectroscopy (FS-CRDS) [56,57]; we use here an experimental profile described in [43]. The spectrum was recorded at a pressure of 933 Pa (7 Torr) with SNR of 220 000. It was measured in $T = 295.5$ K; hence for all fits from Figs. 3(b)–3(j) the Doppler broadening ω_D was fixed to 570.02 MHz. Moreover, this spectrum, beyond the absorption line profile [Eq. (2)], contains also a very small $A_{\text{etal}} \sin(\frac{2\pi}{\Omega_{\text{etal}}}\omega + \phi_{\text{etal}})$ -type contribution coming from the etaloning effects [43,58]. Following [43], we assumed that the period of this oscillation is equal to 4.5 GHz. We found that the best fit was achieved for $A_{\text{etal}} = -0.000\,072\,835 \times 10^{-6} \text{ cm}^{-1}$ and $\phi_{\text{etal}} = -1.199\,66$ in the case of SD_hB₁₂P. The same values of these parameters were used as fixed in fitting all line profiles shown in Figs. 3(b)–3(j).

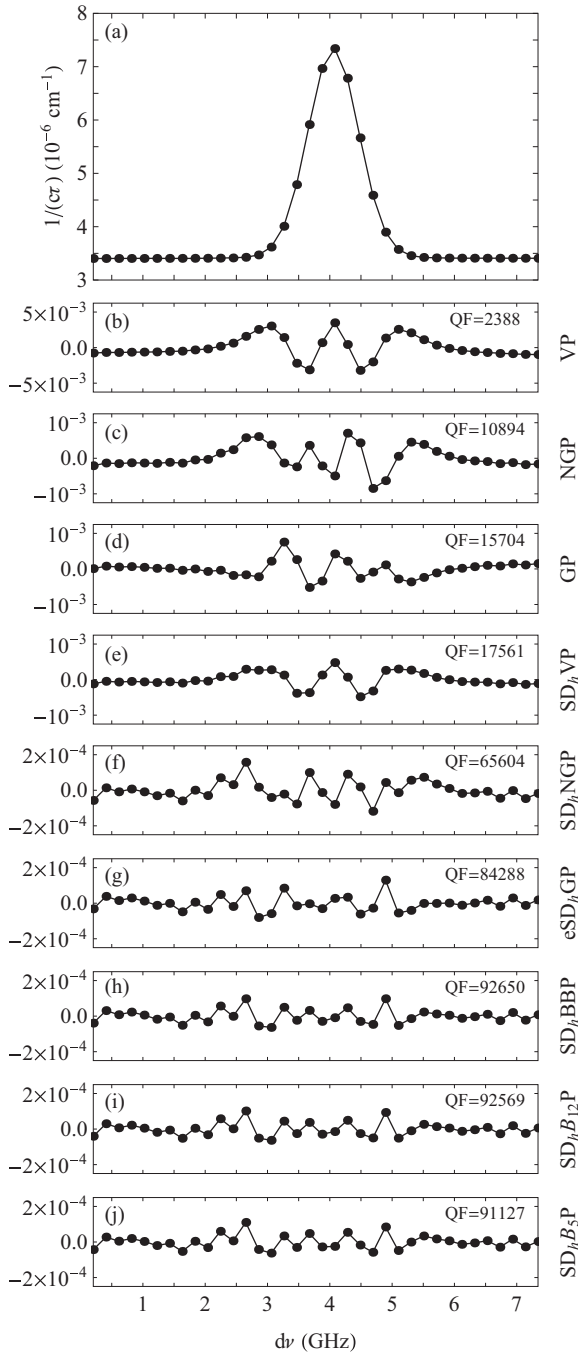


FIG. 3. (a) Spectral line profile of the $^{16}\text{O}_2$ B-band rovibronic transitions measured with a PDH-locked FS-CRDS spectrometer [43] at a pressure of 933 Pa. Charts (b)–(j) show the residuals from VP, NGP, GP, SD_hVP , SD_hNGP , eSD_hGP , SD_hBBP , $\text{SD}_h\text{B}_{12}\text{P}$, and $\text{SD}_h\text{B}_5\text{P}$, respectively. All fitted profiles were generated for $N_{\max} = L_{\max} = K_{\max} = 25$ with fixed Doppler broadening $\omega_D = 570.02$ MHz corresponding to the temperature of 295.5 K.

We take advantage of the wide variety of line-shape models to test which one is best able to reproduce the experimental spectrum. Following [43], to express fit quality quantitatively, we defined a quality of the fit parameter

$$\text{QF} = (\alpha_{\max} - \alpha_{\min}) / \tilde{S}_R, \quad (14)$$

where \tilde{S}_R is the standard deviation of fit residuals calculated as

$$\tilde{S}_R = \sqrt{\frac{1}{M-k} \sum_{i=1}^M [\alpha_{\text{expt}}(v_i) - \alpha_{\text{fit}}(v_i)]^2}, \quad (15)$$

where M is a number of points in the profile, k is a number of fitted parameters, and $\alpha_{\text{expt}}(v_i)$ and $\alpha_{\text{fit}}(v_i)$ are experimental and fitted absorption coefficients, respectively. The sum of the baseline level of the absorption spectrum α_{\min} and the maximum absorption coefficient is denoted as α_{\max} . The QF parameter can be interpreted as a SNR with which a line shape is fitted to experimental data.

It should be mentioned that in [43], by mistake, the value of k [Eq. (15)] was set to 1 instead of to the number of fitted parameters, so the values of QF from [43] should be multiplied by $\sqrt{(M-k)/(M-1)}$. Moreover, in [43] the etalon parameters were fitted for each of the considered profiles independently, in contrast to this model. Nevertheless, comparison of fitting results for $\text{SD}_h\text{B}_{12}\text{P}$ with those shown in [43] demonstrates superiority of the $\text{SD}_h\text{B}_{12}\text{P}$ and SD_hBBP model over all other models used in [43].

Figure 3(b) shows the residuals from a simple Voigt profile (VP), which takes into account only Doppler broadening and speed-independent dephasing collisions. In this case five parameters were fitted ($k = 5$): profile area A , pressure broadening Γ (half width at half maximum), transition frequency ω_0 , and baseline offset and slope. Evidently, VP is not able to reproduce the experimental spectrum, since the residuals from it forms a clear structure (QF = 2388). Values of the fitted parameters are summarized in Table I. Much better agreement with the measured spectrum may be achieved when the line-shape model allows us to handle also a Dicke narrowing effect [59,60]. In the simplest cases it can be realized with the Nelkin-Ghatak profile (NGP) accounting from the hard-collisions model [61,62] and with the Galatry profile (GP) accounting from the soft-collisions model [62,63]. Residuals from NGP and GP are shown in Figs. 3(c) and 3(d), respectively (here $k = 6$, since also frequency of optical velocity-changing collisions ν_{opt} was fitted). The shapes of residuals from NGP and GP are significantly different as it was earlier observed by Triki *et al.* [41] in the low-pressure studies related to the Boltzmann constant determination. Further improvement of consistency with an experiment may be done by introducing the speed-dependent pressure broadening and shifting; see Fig. 3(e) for residuals from the speed-dependent Voigt profile (SD_hVP), Fig. 3(f) for residuals from the speed-dependent Nelkin-Ghatak profile (SD_hNGP) [2], and Fig. 3(g) for residuals from the exact speed-dependent Galatry profile (eSD_hGP) [14]. The h subscript indicates that the hypergeometric speed dependency was taken (here, we chose the exponent from the inverse-power potential $\nu = 5$ describing quadrupole-quadrupole interaction and mass ratio $\alpha = 1$). Introducing the speed dependency the set of fitted parameters was extended by speed-dependent pressure shift Δ , and hence for SD_hVP $k = 6$ and for SD_hNGP and eSD_hGP $k = 7$. A dramatic increase, by more than 27 times, of the quality of fit (QF) from VP [Fig. 3(b)], through NGP [Fig. 3(c)], to SD_hNGP [Fig. 3(f)] was clearly expected, since at each step a qualitatively new mechanism affecting the

TABLE I. Model parameters retrieved from fits to experimental data. The Doppler broadening was set to $\omega_D = 570.02$ MHz, since the measurement was performed in $T = 295.5$ K.

Line profile	QF	A (kHz/cm)	ν_{opt} (MHz)	Γ (MHz)	Δ (MHz)	ω_0 (MHz)
VP	2388	4.0644(21)		11.15(26)	−1.042(fixed)	4058.31(13)
NGP	108 94	4.071 84(54)	2.291(93)	12.718(86)	−1.042(fixed)	4058.311(28)
GP	157 04	4.075 06(43)	4.883(135)	13.525(77)	−1.042(fixed)	4058.313(20)
SD_h VP	175 61	4.072 73(30)		12.960(41)	−1.06(28)	4058.25(26)
SD_h NGP	656 04	4.073 61(9)	0.273(14)	13.152(15)	−1.045(76)	4058.243(71)
SD_h GP	842 88	4.073 98(8)	0.555(22)	13.247(14)	−1.041(59)	4058.239(55)
SD_h BBP	92 650	4.073 87(7)	0.445(16)	13.218(12)	−1.042(54)	4058.240(50)
SD_h B ₁₂ P	925 69	4.073 85(7)	0.437(15)	13.213(12)	−1.042(54)	4058.240(50)
SD_h B ₅ P	911 27	4.073 82(7)	0.412(15)	13.204(12)	−1.042(55)	4058.240(51)

line profile and related with it a new parameter to fit were introduced. Much more subtle effects explain the increase of QF from Figs. 3(f) to 3(h). For all from these three profiles both Dicke narrowing and speed-dependent effects were included. They differ only by the description of the mechanism of the velocity-changing collisions leading to the Dicke narrowing. The hard collisions model is only a simple phenomenological approach to velocity-changing collisions and consequently SD_h NGP does not reproduce the measured spectrum accurately. Much better description (with QF higher by almost 30%) is provided by a soft collisions model, where perturbers are assumed to be infinitesimally light. Further increase of QF by about 10% was obtained by taking advantage of the speed-dependent billiard-balls profile (SD_h BBP) [14], see also Refs. [25–31], which allows us to set an exact perturber to absorber mass ratio α (here, for O₂-O₂ collisions $\alpha = 1$); see Fig. 3(h). It is noteworthy that the improvement of the QF by more than 40% from SD_h NGP [Fig. 3(f)], through eSD_h GP [Fig. 3(g)], to SD_h BBP [Fig. 3(h)] was obtained for the same set of fitted parameters ($k = 7$).

We also checked how the shape of the interaction potential related to velocity-changing collisions influence the quality of fit. To investigate, we applied the speed-dependent Blackmore profile (SD_h B _{ν} P) [10,15,17] accounting from a model $r^{-\nu}$ -type potential describing velocity-changing collisions. Figures 3(h)–3(j) show residuals from SD_h B _{ν} P for $\nu = \infty, 12$, and 5, respectively (note that the billiard-ball profile is a limit case of the Blackmore profile for $\nu \rightarrow \infty$). The quality of the fit (QF) is almost the same for $\nu = \infty$ and 12, while for $\nu = 5$ is slightly smaller (by about 1.5%). For all these three profiles the number of fitted parameters was set to $k = 7$. Moreover, from the point of view of an accurate gas metrology, an error caused by improper choice of model of potential related to velocity-changing collisions can be estimated by comparing values of the fitted parameters. For instance discrepancies of the determination of the pressure broadening Γ coefficient are of the order of 0.1%; see Table I. However, for the narrowing parameter ν_{opt} these discrepancies were even as high as 7%.

Lack of knowledge of real collisional operator \hat{S}^f can lead to systematic errors in the determination of fitted line-shape parameters. These errors can be minimized by calculating the \hat{S}^f collisional operator from the *ab initio* potential surfaces solving the close-coupled scattering equations. However, it is out of the scope of this paper. Nevertheless, it should be noted

that the simplifications in the assumed here description of velocity-changing collisions and speed-dependent collisional broadening and shifting can lead to some systematic errors exceeding small statistical uncertainties reported here. One way of future quantification of the above-mentioned systematic errors can be a comparison with the *ab initio* line-shape calculations based on the molecular dynamics simulations (MDS) [64,65] in the wide range of perturber pressures.

To qualify how the choice of the line-shape model can affect the Doppler-width thermometry [35–41], we fitted our experimental data with analytical SD_h NGP and numerical SD_h BBP allowing variation of the Doppler width ω_D . The Doppler widths ω_D determined from the fit of SD_h NGP and SD_h BBP are equal to 569.826(14) MHz and 569.992(66) MHz, respectively. The use of SD_h NGP can lead to systematic reduction of Doppler width determination by 166 kHz with respect to SD_h BBP. It corresponds to the 3×10^{-4} fraction of the Doppler width ω_D . Clearly, the use of SD_h BBP or SD_h B _{ν} P can help reduce the systematic errors in determination of the Boltzmann constant. These results can be important for optical determination of the Boltzmann constant recently reported by Moretti *et al.* [42].

Finally, we investigated how the proper choice of the line-shape model affects the statistical uncertainties of determined unperturbed transition frequency ω_0 . In general, this precision grows up with the growth of the quality of fit (QF). However, comparing the ω_0 uncertainties from Table I, one may observe that for the speed-dependent profiles the ω_0 uncertainty is larger than for speed-independent ones. It is caused by strong correlation between the line shift Δ and the unperturbed transition frequency ω_0 . In fact, the position of the line is determined much more precisely than uncertainty indicated in Table I. The impact of this correlation can be reduced significantly by simultaneously fitting several spectra for different pressures. To estimate how high precisions of the spectral line position can be achieved, we repeated the fitting procedure for the SD_h BBP case fixing the line shift Δ and we obtained the statistical uncertainty of 3 kHz. Determination of spectral line positions in Doppler limited spectroscopy with kilohertz accuracy combined with optical frequency comb reference [49,50,66] can have an impact on fundamental research in molecular physics [47,67,68] for which the proper line-shape analysis will be crucial, as it was demonstrated earlier [69] for less precise data.

VI. CONCLUSIONS

In this paper the problem of the line-shape profiles determination, within the impact approximation, for a wide range of pressures down to the Doppler limit was addressed. It was shown that the iterative approach to the transport-relaxation equation can be modified such as to be applicable also for very low pressures. In contrast to the previous analysis [14,22,28,31,32] it was demonstrated that the decomposition of functions and operators in the Burnett basis can be efficiently applied to the transport-relaxation equation also for the low pressure range. This decomposition allows us to convert the transport-relaxation equation (which is an integral equation) into a simple algebraic recursive formula. It was presented that for various line-shape models the relative accuracy of this technique is better than 10^{-7} (for the Burnett basis dimensions $N_{\max} = L_{\max} = 25$). Finally, it was shown that this iterative technique together with an appropriate line-shape model is able to reproduce a high-quality experimental data with relative accuracy of the order of 10^{-5} .

The data analysis technique presented here together with ultraprecise experimental spectra can lead to determination of molecular transition frequencies with accuracy approaching kilohertz level in the Doppler limited spectroscopy. Moreover, the ability of the line-shape calculations, *ab initio* in spirit, at low pressures down to the Doppler limit allows reduction of systematic errors in spectroscopic Boltzmann constant determination.

ACKNOWLEDGMENTS

The authors would like to thank L. Gianfrani for sending the paper [42] before publication. The research is a part of the program of the National Laboratory FAMO in Toruń, Poland. The research is partially supported by the Foundation for Polish Science TEAM Project cofinanced by the EU European Regional Development Fund, and is partially supported by the National Science Centre, Project No. DEC-2011/01/B/ST2/00491. A.C. is partially supported by the Foundation for Polish Science START Project.

-
- [1] P. Duggan, P. M. Sinclair, A. D. May, and J. R. Drummond, *Phys. Rev. A* **51**, 218 (1995).
- [2] B. Lance, G. Blanquet, J. Walrand, and J. P. Bouanich, *J. Mol. Spectrosc.* **185**, 262 (1997).
- [3] R. Ciuryło, *Phys. Rev. A* **58**, 1029 (1998).
- [4] B. Lance and D. Robert, *J. Chem. Phys.* **109**, 8283 (1998); **111**, 789 (1999).
- [5] A. S. Pine, *J. Quant. Spectrosc. Radiat. Transfer* **62**, 397 (1999).
- [6] D. Priem, F. Rohart, J.-M. Colmont, G. Włodarczak, and J.-P. Bouanich, *J. Mol. Struct.* **517-518**, 435 (2000).
- [7] R. Ciuryło, A. S. Pine, and J. Szudy, *J. Quant. Spectrosc. Radiat. Transfer* **68**, 257 (2001).
- [8] J.-M. Hartmann, C. Boulet, and D. Robert, *Collisional Effects on Molecular Spectra* (Elsevier, Amsterdam, 2008).
- [9] P. R. Berman, J. E. M. Haverkort, and J. P. Woerdman, *Phys. Rev. A* **34**, 4647 (1986).
- [10] R. Blackmore, *J. Chem. Phys.* **87**, 791 (1987).
- [11] R. Blackmore, S. Green, and L. Monchick, *J. Chem. Phys.* **91**, 3846 (1989).
- [12] G. L. Rogers and P. R. Berman, *Phys. Rev. A* **44**, 417 (1991).
- [13] D. A. Shapiro, R. Ciuryło, J. R. Drummond, and A. D. May, *Phys. Rev. A* **65**, 012501 (2002).
- [14] R. Ciuryło, D. A. Shapiro, J. R. Drummond, and A. D. May, *Phys. Rev. A* **65**, 012502 (2002).
- [15] P. Wcisło and R. Ciuryło, *J. Phys.: Conf. Ser.* **397**, 012008 (2012).
- [16] A. D. May, W.-K. Liu, F. R. W. McCourt, R. Ciuryło, J. Sanchez-Fortún Stoker, D. Shapiro, and R. Wehr, *Can. J. Phys.* (2013), doi: 10.1139/cjp-2012-0345.
- [17] P. Wcisło and R. Ciuryło, *J. Quant. Spectrosc. Radiat. Transfer* **120**, 36 (2013).
- [18] D. A. Shapiro, R. Ciuryło, R. Jaworski, and A. D. May, *Can. J. Phys.* **79**, 1209 (2001).
- [19] H. Tran and J.-M. Hartmann, *J. Chem. Phys.* **130**, 094301 (2009).
- [20] H. Tran, J.-M. Hartmann, F. Chaussard, and M. Gupta, *J. Chem. Phys.* **131**, 154303 (2009).
- [21] H. Tran, N. H. Ngo, J.-M. Hartmann, R. R. Gamache, D. Mondelain, S. Kassi, A. Campargue, L. Gianfrani, A. Castrillo, E. Fasci, and F. Rohart, *J. Chem. Phys.* **138**, 034302 (2013).
- [22] M. J. Lindenfeld, *J. Chem. Phys.* **73**, 5817 (1980).
- [23] D. Robert and L. Bonamy, *Eur. Phys. J. D* **2**, 245 (1998).
- [24] L. Bonamy, H. Tran, Thi Ngoc, P. Jouberta, and D. Robert, *Eur. Phys. J. D* **31**, 459 (2004).
- [25] R. Wehr, A. Vitcu, R. Ciuryło, F. Thibault, J. R. Drummond, and A. D. May, *Phys. Rev. A* **66**, 062502 (2002).
- [26] R. Ciuryło, D. Lisak, and J. Szudy, *Phys. Rev. A* **66**, 032701 (2002).
- [27] R. Ciuryło, A. Bielski, J. R. Drummond, D. Lisak, A. D. May, A. S. Pine, D. A. Shapiro, J. Szudy, and R. S. Trawiński, in *Spectral Line Shapes*, edited by C. A. Back (AIP, Melville, NY, 2002), p. 151.
- [28] D. Lisak, A. Bielski, R. Ciuryło, J. Domysławska, R. S. Trawiński, and J. Szudy, *J. Phys. B: At. Mol. Opt. Phys.* **36**, 3985 (2003).
- [29] R. Wehr, R. Ciuryło, A. Vitcu, F. Thibault, J. R. Drummond, and A. D. May, *J. Mol. Spectrosc.* **235**, 54 (2006).
- [30] R. Wehr, A. Vitcu, F. Thibault, J. R. Drummond, and A. D. May, *J. Mol. Spectrosc.* **235**, 69 (2006).
- [31] D. Lisak, J. T. Hodges, and R. Ciuryło, *Phys. Rev. A* **73**, 012507 (2006).
- [32] D. A. Shapiro and A. D. May, *Phys. Rev. A* **63**, 012701 (2000).
- [33] G. Nienhuis, *J. Quant. Spectrosc. Radiat. Transfer* **20**, 275 (1978).
- [34] S. Dolbeau, R. Berman, J. R. Drummond, and A. D. May, *Phys. Rev. A* **59**, 3506 (1999).
- [35] K. M. T. Yamada, A. Onae, F.-L. Hong, H. Inaba, and T. Shimizu, *C. R. Phys.* **10**, 907 (2009).

- [36] A. Castrillo, M. D. De Vizia, L. Moretti, G. Galzerano, P. Laporta, A. Merlone, and L. Gianfrani, *Phys. Rev. A* **84**, 032510 (2011).
- [37] C. Lemarchand, M. Triki, B. Darquie, Ch. J. Borde, C. Chardonnet, and C. Daussy, *New J. Phys.* **13**, 073028 (2011).
- [38] Y. R. Sun, H. Pan, C.-F. Cheng, A.-W. Liu, J.-T. Zhang, and S.-M. Hu, *Opt. Express* **19**, 19993 (2011).
- [39] A. Cygan, D. Lisak, R. S. Trawiński, and R. Ciuryło, *Phys. Rev. A* **82**, 032515 (2010).
- [40] M. D. De Vizia, L. Moretti, A. Castrillo, E. Fasci, and L. Gianfrani, *Mol. Phys.* **109**, 2291 (2011).
- [41] M. Triki, C. Lemarchand, B. Darquie, P. L. T. Sow, V. Roncin, C. Chardonnet, and C. Daussy, *Phys. Rev. A* **85**, 062510 (2012).
- [42] L. Moretti, A. Castrillo, E. Fasci, M. D. De Vizia, G. Casa, G. Galzerano, A. Merlone, P. Laporta, and L. Gianfrani [Phys. Rev. Lett. (to be published)].
- [43] A. Cygan, D. Lisak, S. Wójtewicz, J. Domysławska, J. T. Hodges, R. S. Trawiński, and R. Ciuryło, *Phys. Rev. A* **85**, 022508 (2012).
- [44] D. A. Long, D. K. Havey, M. Okumura, H. M. Pickett, C. E. Miller, and J. T. Hodges, *Phys. Rev. A* **80**, 042513 (2009).
- [45] D. A. Long, M. Okumura, C. E. Miller, and J. T. Hodges, *Appl. Phys. B* **105**, 471 (2011).
- [46] M. D. De Vizia, F. Rohart, A. Castrillo, E. Fasci, L. Moretti, and L. Gianfrani, *Phys. Rev. A* **83**, 052506 (2011).
- [47] S. Kassi, A. Campargue, K. Pachucki, and J. Komasa, *J. Chem. Phys.* **136**, 184309 (2012).
- [48] S. Kassi and A. Campargue, *J. Chem. Phys.* **137**, 234201 (2012).
- [49] J. Domysławska, S. Wójtewicz, D. Lisak, A. Cygan, F. Ozimek, K. Stec, Cz. Radzewicz, R. S. Trawiński, and R. Ciuryło, *J. Chem. Phys.* **136**, 024201 (2012).
- [50] G.-W. Truong, D. A. Long, A. Cygan, D. Lisak, R. D. van Zee, and J. T. Hodges, *J. Chem. Phys.* **138**, 094201 (2013).
- [51] A. D. May, *Phys. Rev. A* **59**, 3495 (1999).
- [52] M. J. Lindenfeld and B. Shizgal, *Chem. Phys.* **41**, 81 (1979).
- [53] P. R. Berman, *J. Quant. Spectrosc. Radiat. Transfer* **12**, 1331 (1972).
- [54] R. Ciuryło, R. Jaworski, J. Jurkowski, A. S. Pine, and J. Szudy, *Phys. Rev. A* **63**, 032507 (2001).
- [55] C. D. Boone, K. A. Walker, and P. F. Bernath, *J. Quant. Spectrosc. Radiat. Transfer* **105**, 525 (2007).
- [56] A. Cygan, D. Lisak, P. Masłowski, K. Bielska, S. Wójtewicz, J. Domysławska, R. S. Trawiński, R. Ciuryło, H. Abe, and J. T. Hodges, *Rev. Sci. Instrum.* **82**, 063107 (2011).
- [57] A. Cygan, D. Lisak, S. Wójtewicz, J. Domysławska, R. S. Trawiński, and R. Ciuryło, *Meas. Sci. Technol.* **22**, 115303 (2011).
- [58] S. Kassi, D. Romanini, A. Campargue, and B. Bussery-Honvault, *Chem. Phys. Lett.* **409**, 281 (2005).
- [59] R. H. Dicke, *Phys. Rev.* **89**, 472 (1953).
- [60] J. P. Wittke and R. H. Dicke, *Phys. Rev.* **103**, 620 (1956).
- [61] M. Nelkin and A. Ghatak, *Phys. Rev.* **135**, A4 (1964).
- [62] S. G. Rautian and I. I. Sobelman, *Usp. Fiz. Nauk* **90**, 209 (1966); *Sov. Phys. Usp.* **9**, 701 (1967).
- [63] L. Galatry, *Phys. Rev.* **122**, 1218 (1961).
- [64] J.-M. Hartmann, V. Sironneau, C. Boulet, T. Svensson, J. T. Hodges, and C. T. Xu, *Phys. Rev. A* **87**, 032510 (2013).
- [65] J.-M. Hartmann, H. Tran, N. H. Ngo, X. Landsheere, P. Chelin, Y. Lu, A.-W. Liu, S.-M. Hu, L. Gianfrani, G. Casa, A. Castrillo, M. Lepere, Q. Deliere, M. Dhyne, and L. Fissiaux, *Phys. Rev. A* **87**, 013403 (2013).
- [66] G. Galzerano, A. Gambetta, E. Fasci, A. Castrillo, M. Marangoni, P. Laporta *et al.*, *Appl. Phys. B* **102**, 725 (2011).
- [67] E. J. Salumbides, J. C. J. Koelemeij, J. Komasa, K. Pachucki, K. S. E. Eikema, and W. Ubachs, [arXiv:1304.6560](https://arxiv.org/abs/1304.6560).
- [68] G. D. Dickenson, M. L. Niu, E. J. Salumbides, J. Komasa, K. S. E. Eikema, K. Pachucki, and W. Ubachs, *Phys. Rev. Lett.* **110**, 193601 (2013).
- [69] P. M. Sinclair, J. Ph. Berger, X. Michaut, R. Saint-Loup, R. Chaux, H. Berger, J. Bonamy, and D. Robert, *Phys. Rev. A* **54**, 402 (1996).